

UV spectroscopic determination of the chlorine monoxide (ClO) / chlorine peroxide (ClOOCl) thermal equilibrium constant

J. Eric Klobas¹ and David M. Wilmouth¹

¹Harvard John A. Paulson School of Engineering and Applied Sciences and Department of Chemistry and Chemical Biology, Harvard University, Cambridge, MA 02138, USA

Correspondence: J. Eric Klobas (klobas@huarp.harvard.edu)

Abstract. The thermal equilibrium constant between the chlorine monoxide radical (ClO) and its dimer, chlorine peroxide (ClOOCl), was determined as a function of temperature between 228 – 301 K in a discharge flow apparatus using broadband UV absorption spectroscopy. A third law fit of the equilibrium values determined from the experimental data provides the expression: $K_{\text{eq}} = 2.16 \times 10^{-27} e^{(8527 \pm 35 \text{ K}/T)} \text{ cm}^3 \text{ molecule}^{-1}$ (1σ uncertainty). A second law analysis of the data is in good agreement. From the slope of the van't Hoff plot in the third law analysis, the enthalpy of formation for ClOOCl is calculated, $\Delta H_f^\circ(298 \text{ K}) = 130.0 \pm 0.6 \text{ kJ mol}^{-1}$. The equilibrium constant results from this study suggest that the uncertainties in K_{eq} recommended in the most recent (year 2015) NASA JPL Data Evaluation can be significantly reduced.

1 Introduction

Halogen-mediated catalytic processing of ozone accounts for the overwhelming majority of lower stratospheric ozone-loss processes in polar winter and spring (e.g., WMO, 2014; Wilmouth et al., 2018). Approximately half of this loss (Wohlmann et al., 2017) is resultant from the ClO dimer cycle (Molina and Molina, 1987), which occurs as a result of the highly perturbed physicochemical conditions of the polar vortices:





Within this cycle, the equilibrium governing the partitioning of ClO and ClOOCl in reaction (R1) is defined as:

$$K_{\text{eq}} = \frac{[\text{ClOOCl}]}{[\text{ClO}]^2} \quad (1)$$

- 5 This thermal equilibrium is a key parameter that determines the nighttime partitioning of active chlorine in the winter-spring polar vortex. The value of K_{eq} can also tune the efficiency of chlorine-mediated ozone destruction, particularly the radial extent of ozone loss within the warmer Arctic polar vortex. For example, Canty et al. (2016) quantified how small variations in K_{eq} can modulate significant changes in the temperature at which photolysis of ClOOCl and thermal decomposition of ClOOCl occur at equal rates.
- 10 Although the partitioning between ClO and ClOOCl is highly important, relatively few laboratory measurements of K_{eq} have been made, and there is significant disagreement between reported values. Accordingly, the uncertainty in K_{eq} was large (e.g., ~75% at 200 K) as of the 2011 JPL compendium recommendation (Sander et al., 2011). The most recent 2015 JPL-recommended value of K_{eq} was revised on the basis of a 2015 study by Hume et al. (2015), but the recommended uncertainties are still substantial—exceeding 50% at 200 K (Burkholder et al., 2015).
- 15 The preponderance of laboratory data from previous determinations of K_{eq} was obtained at temperatures significantly warmer than the polar stratosphere ($T > 250$ K). Error in the extrapolation of these warm temperature data has often been cited to explain the lack of correspondence between values of K_{eq} determined in the laboratory and those calculated from stratospheric observations (Avalone and Toohey, 2001; Stimpfle et al., 2004; von Hobe et al., 2005; Santee et al., 2010). The more recent results of Hume et al. (2015) are unique in that they were obtained at temperatures colder than other laboratory
- 20 studies ($206 \text{ K} < T < 250 \text{ K}$), but their experimental method was compromised by secondary bimolecular reactions at warmer temperatures. In the present study, our spectroscopic data bridge the warmer temperatures where most laboratory determinations of K_{eq} have been made to the colder temperature work of Hume et al. (2015), covering a broader temperature range than any previous study. The thermal equilibrium constant between ClO and ClOOCl was measured as a function of temperature ($228 \text{ K} < T < 301 \text{ K}$) by UV spectroscopy and is evaluated here in relation to prior determinations, observations, and
- 25 compendial recommendations.

2 Experimental

- All experiments were conducted in a discharge flow apparatus, as shown in Figure 1. Independently programmable thermal zones allow for the optimization of target chemistry as a function of flow velocity, temperature, and pressure. ClO is synthesized via the reaction of Cl atoms with O₃ (reaction R4). Cl is produced from a 1% Cl₂/He gas mixture, diluted further with UHP
- 30 He and directed through a 45 W, 2.45 GHz microwave discharge. O₃ is produced via electric discharge of a 10% O₂/Ar source mixture and subsequently introduced 2.5 cm after the microwave cavity. Once formed, ClO readily dimerizes to form ClOOCl (reaction R1), particularly at higher concentrations and colder temperatures.

To facilitate dimerization of ClO, the gas mixture is cooled in a 20-cm long jacketed quartz cell immediately subsequent to the microwave discharge. This reaction cell (Figure 1) has an inner diameter of 1 cm and can be maintained at a temperature between 198 – 305 K via circulating chilled methanol (NESLAB Endocal ULT-80). The operation of this cell at cold temperatures additionally suppresses undesired chemistry, preventing the synthesis of side products such as OCIO per reaction (R6), and subsequently Cl₂O₃ per reaction (R7).



Following the reaction cell, the gas stream then passes through the cold trap zone, which is maintained at temperatures between 100 K and room temperature depending on the experiment. Cooling is accomplished by flowing N₂ gas through a copper coil immersed in liquid N₂ and then through an 18-cm long insulated aluminum jacket surrounding the 1-cm inner diameter quartz flow tube. Type K thermocouples (alumel/chromel) are affixed at three positions on the outside of the flow tube, opposite the cryogenic gas ports. These thermocouples are further insulated to ensure the recorded voltages correspond to the temperature of the quartz tube and not the temperature of the cryogenic gas. The coupling between the cold trap and the equilibrium cell is actually linear but is presented as a right angle in Figure 1 for graphical purposes.

The next section of the flow system in Figure 1, labeled equilibrium cell, is a jacketed 50-cm quartz tube of 1-cm inner diameter. This section is where the gases reach equilibrium prior to measurement in the absorption cell. The equilibrium cell and the absorption cell share a coupled circulating chilled methanol bath (NESLAB ULT-80) ensuring that the two cells are maintained at the same temperature. The equilibrium cell is isolated from the environment with two 10-mm blankets of aerogel insulation (Cryogel Z). Additionally, a flow of cryogenic N₂ passes through an insulated aluminum jacket surrounding the union between the equilibrium cell and the absorption cell. This N₂ is chilled by passing through a copper coil immersed in the reservoir of the circulating chiller servicing the reaction cell, and the flow is modulated to provide constant temperature as the gas mixture transits from the equilibrium cell to the detection axis. A 100 Ω thermistor is inserted into the gas stream at this location to verify the temperature.

Finally, the gas mixture enters the absorption cell, a 91.44-cm jacketed quartz tube with an inner diameter of 2.54 cm. This detection axis is oriented at a right angle to the equilibrium cell and is terminated with two quartz windows. A 100 Ω thermistor is positioned at the halfway point. Cryogenic circulating methanol provides for temperature control between 228 – 301 K. Two 10-mm blankets of aerogel insulation (Cryogel Z) provide thermal isolation from the environment. An exterior dry N₂ purge is employed to prevent window condensation.

The discharge reactor is operated at pressures between 100 – 333 mbar. Pressure is monitored with Baratron capacitance manometers. Carrier gas flow rates, ~1.0 – 1.8 L min⁻¹ depending on the experimental conditions, are metered via MKS mass flow controllers. Cl₂ flow rates are controlled via a needle valve, while O₃ addition is modulated using micrometer flow

control valves. Total system pressure and velocity are tuned using an integral bonnet needle valve. Residence times within the absorption cell range between $\sim 1 - 11$ seconds, depending on gas flow rates, system temperature, and pressure. A quarter-turn plug valve provides a bypass of the integral bonnet needle valve such that rapid pump down of the reactor and reignition of the plasma can be performed without disturbing pressure calibration during the course of experiments.

5 Data were acquired using a fiber-coupled Ocean Optics USB4000 UV-Vis spectrometer (~ 0.3 nm resolution) illuminated by a Hamamatsu L2D2 deuterium lamp. The need to correlate Baratron, thermocouple, and thermistor sensor readings with each UV spectrum required the in-house development of custom software. Drivers and libraries to operate the spectrometer and simultaneously interrogate analog sensors were written in Python 2.7 and, in combination with the Python-Seabreeze library, provided scriptable, automated control of nearly all aspects of the data acquisition system.

10 The deuterium lamp was allowed to warm up for at least one hour prior to data collection activity to reduce small variations in lamp output on experimental timescales. Dark spectra were acquired prior to any experiments on a daily basis. Background spectra were obtained with the microwave plasma extinguished and all gas flows of species that absorb in the region of 200 – 295 nm (e.g. O_3 , Cl_2) off. For consistency, sample spectra were obtained exactly 100 seconds after the background spectra against which they were referenced. Each saved spectrum consists of the coaddition of 597 individual scans, the number of
15 scans that could be obtained in exactly 3 minutes of acquisition time.

To aid in the selection of experimental conditions, a simulation of the discharge-flow reactor was constructed. A numerical integrator for chemical kinetics (written in Python 2.7 with NumPy and SciPy) for 18 chemical species and 45 relevant chemical reactions was informed by JPL Data Evaluation 15-10 kinetic rate constants (Burkholder et al., 2015) and coupled into a physical model of gas flows as a function of reactor geometry, temperature, and pressure. Temperature and pressure ranges
20 were scanned to determine optimal conditions to ensure ClO-ClOOCl equilibrium within the real-world experiment. Because parameterized simulations carry inherent uncertainty, experimental conditions were selected at several pressures along the equilibrium asymptote (K_{eq} vs P), and real-world experiments were performed at pressures above and below the identified value in order to confirm asymptotic equilibrium behavior. The kinetic model was only used to inform conditions for the experimental setup, but no results from the model were used in the determination of the reported equilibrium constants.

25 3 Results and Discussion

More than 136,000 background and sample spectra were obtained between the temperatures of 228 – 301 K at pressures ranging between 100 – 333 mbar. Typical initial concentrations spanned $2 \times 10^{13} - 4 \times 10^{14}$ molecules cm^{-3} for O_3 and $1 \times 10^{14} - 4 \times 10^{15}$ molecules cm^{-3} for Cl_2 . Active chlorine (ClO_x) concentrations were typically $1 \times 10^{13} - 1 \times 10^{14}$ molecules cm^{-3} with the microwave discharge on. These values were tuned according to the initial conditions prescribed by the model simu-
30 lations, as described above. For example, as the target temperature of the experiment decreased, the system was operated at incrementally higher pressures to allow more time for equilibrium to be achieved. Higher temperature samples reached equilibrium more readily, so gas velocity was increased to limit the impact of enhanced rates of secondary chemistry on observed K_{eq} values.

Multicomponent spectral curve fitting software packages were programmed in Python 2.7/LmFit (Newville et al., 2016) for the deconvolution of the UV absorption spectra of O₃, Cl₂, ClO, ClOOCl, OCIO, and Cl₂O₃. Reference cross sections were utilized as follows: For O₃ and OCIO, pure sample spectra were acquired and scaled to match the 2015 JPL-recommended cross sections of Molina and Molina (1986) and Kromminga et al. (2003), respectively. ClOOCl and Cl₂O₃ cross sections were obtained directly from the 2015 JPL data evaluation (Burkholder et al., 2015). Temperature-dependent cross sections of Cl₂ were obtained from Marić et al. (1993) and validated to match observed Cl₂ spectra along the experimental temperature range. Synthetic temperature-dependent cross sections from Marić and Burrows (1999) were used for ClO due to the broad temperature range over which the data are available.

The cross sections from Marić and Burrows (1999) were found to provide an excellent fit of experimentally obtained ClO at all relevant temperatures in this study and were validated against available laboratory-determined ClO cross sections from the literature. Our experimental spectra at 263 K fit using both the synthetic ClO cross sections of Marić and Burrows (1999) and the reported experimental cross sections of Trolier et al. (1990) at 263 K result in concentrations of ClO that differ by only 3.0%. Similarly, experimental samples at 300 K from this study fit to the room temperature, laboratory ClO cross sections of Simon et al. (1990) and Sander and Friedl (1988) have excellent correspondence with the synthetic cross sections of Marić and Burrows (1999): 1.1% deviation in ClO concentration in comparison with Simon et al. (1990) and 2.6% deviation in comparison with Sander and Friedl (1988). The resolution of our experimental spectra was degraded to match the lower resolution data of Trolier et al. (1990) for this comparison, while the cross sections of Sander and Friedl (1988) and Simon et al. (1990), which were published at higher resolution than provided by our spectrometer, were degraded to our spectral resolution.

A total of 82 experimental observations of the equilibrium gas mixture were acquired across a broad range of conditions (e.g., changing initial gas concentrations, pressure, temperature, carrier gas flow rates, or microwave discharge power). Multiple observations acquired under the same experimental conditions were reduced to a single measurement by coaddition of spectra. Samples at colder temperatures were subjected to more repeated evaluations to improve accuracy under the low ClO conditions.

Concentrations of ClO and ClOOCl were obtained via spectral deconvolution as follows. Quantification of ClO was determined from high pass filtration of each absorbance spectrum to remove the contributions of absorbers that are spectrally smooth. The highly structured vibrational bands of the ClO $A^2\Pi \leftarrow X^2\Pi$ transition were similarly extracted from the ClO reference spectra at the appropriate temperature, and least-squares minimization was conducted in the wavelength region of 260 – 300 nm. ClOOCl was then quantified by multicomponent linear regression, constraining ClO to the previously determined concentration, over the wavelength range of 230 – 260 nm. The custom software used to deconvolve the measured spectra used a differential evolution minimizer via a stochastic process; to test the reproducibility of the deconvolution and to generate fit statistics, each spectral fit was run 100 times. The component gas concentrations for each sample were then determined as the average of the entire deconvolution ensemble for that sample. Though not employed in the calculation of K_{eq} , OCIO was also quantified by spectral deconvolution in the wavelength region of 310 – 350 nm, where instrumental sensitivity to OCIO is maximized. Only in three experimental runs, at temperatures of 294 K and above, was the concentration of OCIO greater than the concentration of the two species of interest – and even then, not by a large margin. Cl₂O₃ was below the detection limit for all spectra collected in this study. The resulting concentrations of ClO, ClOOCl, and OCIO are enumerated in Table 1. Also

shown are the uncertainties (1σ) for each component determined from the spectral fitting procedure, which do not exceed 8% for ClO and 18% for ClOOCl, and in most cases are $< 2\%$ for ClO and $< 5\%$ for ClOOCl. Using the vibrational structure to define the spectral fits for ClO significantly reduces the uncertainty.

Figure 2 demonstrates the fitting process for an experiment conducted at 268.7 K. The raw spectrum and the wavelength regions used to fit each component are presented in panel (a). The colored traces overlapping the raw spectrum show the fit results, with each trace being the sum of the deconvolved components. Additionally, the residual from each fit is shown, offset from the baseline for clarity and provided at 3-times magnification for additional diagnosis of fit quality. Except for a slight deviation in the OCIO fit at the longest wavelengths as a result of source instability in this low light region, the residuals for all three fitting techniques are observed to be flat across the wavelength ranges and minimally structured. This holds true for all spectral fits reported in this work. High pass filtration of ClO is depicted in panel (b) wherein differential absorbance data are plotted with the high pass filtered ClO component from the fit overlaid. The quantification of ClOOCl is presented in panel (c) in which the absorbances of ClOOCl and O_3 are plotted on a log scale for improved visibility, along with the experimental spectrum for reference. Finally, panel (d) shows the OCIO and Cl_2 fitted spectral components between 310 – 350 nm, again plotted on a log scale with the experimental spectrum shown for reference. We note that OCIO is a very small component of the absorbance spectrum and is near the instrumental detection limit, especially in the wavelength regions employed for the quantification of ClO and ClOOCl.

Once the ClO and ClOOCl concentrations are determined from the spectral fit, the value of K_{eq} at the relevant temperature is calculated per equation (1). K_{eq} values for each sample are shown in Table 1 and plotted in Figure 3a as a function of inverse temperature.

The temperature dependence of K_{eq} can be related as an Arrhenius expression, per equation (2), with free parameters A and B .

$$K_{eq} = Ae^{(B/T)} \quad (2)$$

In a third law fit, the prefactor A is fixed to a prescribed value. For this work, we employ the JPL Data Evaluation recommended A parameter value of $2.16 \times 10^{-27} \text{ cm}^3 \text{ molecule}^{-1}$, which is the most recent literature evaluation of this constant (Burkholder et al., 2015). A third law fit of our K_{eq} data yields a B parameter value of 8527 K. This result was obtained by an ordinary least-squares fit of the 82 measurements of K_{eq} (Table 1). The fit is shown in Figure 3a as the black trace. Error from the fitting process was quantified via bootstrapping with 2000 resamplings of the binned K_{eq} results, which establishes a fit error interval of ± 5.2 K. This method only accounts for the fit error and does not take into account other potential sources of experimental error, as discussed below.

The accuracy of the spectral deconvolution demonstrated a temperature dependence due to ClO or ClOOCl concentrations approaching their experimental limit of quantification (ClO limiting measurements at colder temperatures and ClOOCl at warmer temperatures). There is also the potential for secondary chemistry to impact the K_{eq} results, particularly at warmer temperatures (R6). To assess the significance of these temperature dependent factors, least squares third law fits were performed

on sub-sampled data populations. Specifically, an analysis of K_{eq} results obtained between 250 – 301 K, 228 – 291 K, and 250 – 291 K resulted in B parameters of 8531 K, 8525 K, and 8530 K, respectively, which are in excellent agreement with the parameter of 8527 K obtained from a fit of the entire temperature range. The extrapolated value of K_{eq} at 200 K obtained from these sub-sampled datasets varies by $< 3\%$, while at 180 K the spread of the maximal deviation in K_{eq} between subsets is $< 4\%$. An estimate of the third law error from temperature-dependent precision is ± 3 K about the B parameter.

The reproducibility of the B parameter value regardless of the temperature range employed in the spectral fits provides strong evidence that secondary chemistry does not significantly impact the K_{eq} values reported here. To further confirm this result, least squares third law fits were performed separately on all of the experimental runs in Table 1 in which OCIO concentrations were large enough to be quantified and on all of the runs in Table 1 in which OCIO concentrations were below our limit of detection. The resulting B values with and without OCIO are essentially identical, 8526 K and 8527 K, respectively.

Variation in the reference cross section of one component in a multicomponent fit may impact the quality of fit for the other spectral components. It is the trend in the literature to not explicitly include uncertainties from the reference cross sections during assignment of error for K_{eq} ; however, the choice of synthetic cross sections for ClO is considered further here. As discussed, the synthetic temperature-dependent ClO cross sections prepared by Marić and Burrows (1999) were employed for the determination of [ClO] in this study, and the ClO concentrations from fits using these synthetic cross sections differed from ClO concentrations determined using experimentally derived reference standards at most by 3.0%. To capture the uncertainty of this error, all ClO concentrations used to derive K_{eq} were scaled by $\pm 3.0\%$ and then fit by a least-squares third law analysis, producing an estimated error in B due to ClO cross section selection of ± 15 K.

Ultimately, estimating our uncertainty on the B parameter from all known sources of potential error yielded comparable, but smaller, values than simply assigning the error interval such that it fully encompassed $> 68\%$ of the individual K_{eq} results at 1σ . Accordingly, we assign error intervals (1σ) to our B parameter of ± 35 K. Systematic errors arising from experimental design and post-processing technique are estimated to contribute errors that sum to a total smaller than this boundary. The ratio of the individual K_{eq} measurements to the resulting K_{eq} expression from the third law fit is depicted in Figure 3b along with the estimate of error. From this figure, it can be seen that 71% of the individual K_{eq} measurements reside within the 1σ uncertainty interval. The resulting K_{eq} expression from the third law analysis is provided in equation (3).

$$K_{\text{eq}} = 2.16 \times 10^{-27} e^{(8527 \pm 35 \text{ K}/T)} \text{ cm}^3 \text{ molecule}^{-1} \quad (3)$$

Figure 4 provides a comparison of our results to equilibrium constants determined from other laboratory studies. In this and subsequent figures, our data are shown averaged in 3 K intervals, the minimal spacing required to ensure that each data point is averaged with at least one other data point. The presentation of averaged data is for improved figure clarity only; all data analyses were performed with the K_{eq} expression derived from the full data set (equation 3). Notably in Figure 4, the K_{eq} values reported in this work are typically smaller than prior evaluations of K_{eq} at warmer temperatures but match well with the colder temperature observations of Hume et al. (2015) for those data points with overlap (228 – 250 K). Moreover, our third law fit matches well with the results of Hume et al. (2015) when extrapolated to 200 K.

The ratio of K_{eq} values from prior laboratory studies relative to K_{eq} calculated from equation (3) is shown in Figure 5. The 1σ ($B \pm 35$ K) and 2σ ($B \pm 70$ K) error bounds from this work are plotted as shaded gray tones. The K_{eq} values from previous laboratory studies were derived using either UV absorption spectroscopy of equilibrium mixtures of ClO and ClOOCl or by determination of the individual forward and/or reverse kinetic rates of dimerization, reaction (R1). Experimental data from these previous studies are shown as circles and triangles, respectively. As evident in Figure 5, there is much greater variation in the determinations of K_{eq} using kinetics methods.

The experiments of Cox and Hayman (1988) and Hume et al. (2015) were performed by UV analysis. The results of Hume et al. (2015) lie entirely within our 1σ error interval. Though the individual results of Cox and Hayman exhibit significant scatter and some measurements exceed the 2σ error reported here, an ordinary least-squares third law fit of their results using the JPL-recommended A parameter (Burkholder et al., 2015) remains within our 1σ error boundaries ($B = 8537$ K).

Nickolaisen et al. (1994) and Ferracci and Rowley (2010) used flash photolysis/UV absorption spectroscopy to determine the kinetic rates of the individual reactions in order to determine K_{eq} . Though these two studies agree with each other in trend and magnitude, they both exhibit significant departures from our results, possibly due to secondary reactions given the high concentrations of ClO and Cl₂O employed in those studies.

Bröske and Zabel (2006) investigated the kinetics of the ClOOCl dissociation reaction and estimated K_{eq} values using JPL 2002 kinetics (Sander et al., 2003) for the forward reaction (R1). A reanalysis of their results using JPL 2015 kinetics (Burkholder et al., 2015) is plotted as binned averages in Figure 5 (orange triangles, $P < 30$ mbar; brown triangles, $P > 30$ mbar). A reanalysis of the high pressure results of Bröske and Zabel (2006) also provides a third law fit ($K_{\text{eq}} = 2.16 \times 10^{-27} e^{(8498 \text{ K}/T)} \text{ cm}^3 \text{ molecule}^{-1}$) that resides within our 1σ error limits. The discrepancy between the experiments of Bröske and Zabel (2006) conducted at higher pressures and lower pressures is discussed in depth in their work.

Horowitz et al. (1994) examined the loss rate of ClO while monitoring the kinetics and branching ratio of the ClO + ClO reaction and provide a single-point estimate of K_{eq} at 285 K that is within 1σ of the value determined at that temperature in this work. The K_{eq} values of Boakes et al. (2005) using flash photolysis/UV absorption spectroscopy and Ellermann et al. (1995) using pulsed radiolysis/UV absorption spectroscopy lie within our 2σ uncertainty; however, the values of Plenge et al. (2005) via mass spectrometric determination of the ClO-OCl bond strength lie outside the 2σ error limits from this work.

Figure 6 provides a comparison between observational determinations of K_{eq} in the atmosphere and an extrapolation of K_{eq} from this work to 190 K. The determination of K_{eq} by Avallone and Toohey (2001), an analysis of AASE I and AASE II data in which mixing ratios of ClOOCl were inferred from total Cl_y mass conservation rather than directly measured, agree within error with the results of this work. Similarly, a determination of K_{eq} by Santee et al. (2010), informed by ClO mixing ratios retrieved via Aura MLS satellite data and ClOOCl mixing ratios calculated from stratospheric modeling, lies in substantial agreement with the K_{eq} expression derived here. All observed ratios of [ClOOCl] / [ClO]² in the Arctic stratosphere for the nighttime ER-2 flight of 3 Feb 2000 during the SOLVE/THESEO campaign (Stimpfle et al., 2004) also agree within the combined 2σ measurement uncertainties (SOLVE/THESEO measurement uncertainties not plotted for clarity). The K_{eq} expression from von Hobe et al. (2005), which was based on observations in Arctic winter 2003, deviates substantially from K_{eq} determined in this

work; however, von Hobe et al. (2007) postulate that those previous observations of ClO and ClOOCl may not have been in equilibrium and that the ClOOCl measurements may have been biased low.

A thermodynamic representation of parameters A and B [equation (2)] can be obtained from a manipulation of the van't Hoff equation. The prefactor A encodes the standard entropy of reaction change per equation (4), in which the superscript
 5 indicates a standard state of one bar, R' is the gas constant ($83.145 \text{ cm}^3 \text{ bar mol}^{-1} \text{ K}^{-1}$), N_A is Avogadro's constant ($6.0221 \times 10^{23} \text{ molecules mol}^{-1}$), R is the gas constant in energy units ($8.3145 \text{ J mol}^{-1} \text{ K}^{-1}$), e is Euler's number, and T is system temperature.

$$\Delta S^\circ(298 \text{ K}) = R \ln \left(\frac{N_A A}{e R' T} \right) \quad (4)$$

The exponential argument B relates the change in standard enthalpy of reaction as shown in equation (5), with R and T as
 10 defined above.

$$\Delta H^\circ(298 \text{ K}) = -R(T + B) \quad (5)$$

Evaluating equation (5) with our derived value of $B = 8527 \text{ K}$ results in a $\Delta H^\circ(298 \text{ K})$ of $-73.4 \pm 0.6 \text{ kJ mol}^{-1}$ for reaction (R1). The uncertainty estimate on this value was obtained by combining the previously determined uncertainty on our
 15 B parameter ($\pm 35 \text{ K}$) with estimated uncertainties in the reference cross sections for ClOOCl [$\pm 17\%$ variation near the peak cross section at 248 nm, as reported by Lien et al. (2009), Papanastasiou et al. (2009), and Wilmouth et al. (2009)] and for ClO [$\pm 3\%$ variation in the fitted concentrations of ClO between Marić and Burrows (1999), Sander and Friedl (1988), Simon et al. (1990), and Troler et al. (1990)] to produce a possible range in B of 8450 K to 8603 K, as determined from scaled, third law least-squares fits.

Combining our $\Delta H^\circ(298 \text{ K})$ value for reaction (R1) with the JPL-recommended $\Delta H_f^\circ(298 \text{ K})$ for ClO of 101.681 ± 0.040
 20 kJ mol^{-1} (Burkholder et al., 2015) yields a $\Delta H_f^\circ(298 \text{ K})$ for ClOOCl of $130.0 \pm 0.6 \text{ kJ mol}^{-1}$. This result is in excellent agreement with the JPL-recommended value of $130.1 \pm 1 \text{ kJ mol}^{-1}$.

A least-squares second law fit of K_{eq} , in which both A and B are free parameters, yields a determination of K_{eq} as shown in equation (6).

$$K_{\text{eq}} = (2.70 \pm 0.6) \times 10^{-27} e^{(8470 \pm 60 \text{ K}/T)} \text{ cm}^3 \text{ molecule}^{-1} \quad (6)$$

The uncertainties from the second law fit are larger but the results agree well with the third law fit, e.g., agreement to within
 25 3% at 298 K and to within 6% at 200 K. An application of equation (4) to the second law prefactor of $2.70 \times 10^{-27} \text{ cm}^3 \text{ molecule}^{-1}$ produces $\Delta S^\circ(298 \text{ K}) = -145.8 \begin{smallmatrix} +1.7 \\ -2.1 \end{smallmatrix} \text{ J mol}^{-1} \text{ K}^{-1}$ for reaction (R1), which agrees with the JPL-recommended value of $-147.0 \text{ J mol}^{-1} \text{ K}^{-1}$ [calculated from the S values for ClO and ClOOCl in Table 6-2 of Burkholder et al. (2015)]. The value of $\Delta H^\circ(298 \text{ K})$ of $-72.9 \pm 1.0 \text{ kJ mol}^{-1}$ for reaction (R1) from the second law analysis is in good agreement with our
 30 results from the third law analysis.

Notably, the equilibrium constant results obtained in this work agree in trend and magnitude with the recently reported K_{eq} values of Hume et al. (2015). This excellent correspondence is illustrated in Figure 7, in which a least-squares third law fit (with each study weighted equally) is presented for a combined data set containing the results of this work and the work of Hume et al. (2015) in ratio to the current JPL recommendation of $K_{\text{eq}} = 2.16 \times 10^{-27} e^{(8537 \text{ K}/T)} \text{ cm}^3 \text{ molecule}^{-1}$ (Burkholder et al., 2015). The combined works span a temperature range of 206 – 301 K, and the resulting K_{eq} is $2.16 \times 10^{-27} e^{(8532 \text{ K}/T)} \text{ cm}^3 \text{ molecule}^{-1}$. This expression deviates from the JPL-recommended K_{eq} value at 200 K by 2.5%. For illustrative purposes, the uncertainty bounds calculated from this work and the bounds recommended by the current JPL evaluation (Burkholder et al., 2015) are also plotted. Note that all of the plotted data lie within our 1- σ uncertainty; this is because our data are averaged in 3 K intervals here, but our uncertainty was determined from the variance in our full data set (Table 1). The JPL uncertainty, which was not derived from a statistical analysis, but was scaled to encompass the warm temperature results of Cox and Hayman (1988) and Nikolaisen et al. (1994) and the low temperature work of Hume et al. (2015), greatly exceeds the scatter of the individual K_{eq} values from the combined dataset of this work and Hume et al. (2015). Our results suggest that the uncertainties in the current JPL recommendation for K_{eq} can be reduced.

4 Conclusions

The thermal equilibrium governing the association of ClO and dissociation of ClOOCl was investigated in a custom-built discharge-flow reactor by UV spectroscopy between the temperatures of 228 – 301 K. The selected temperature range allowed us to bridge the warmer temperature regime where nearly all previous laboratory studies of K_{eq} have been performed and the recent colder temperature work of Hume et al. (2015). A third law fit of our K_{eq} results deviates from some prior laboratory studies but demonstrates excellent agreement with the work of Hume et al. (2015) and with the currently recommended parameters in the JPL compendium (Burkholder et al., 2015). The agreement between our third law and second law analyses lends further confidence to the results reported herein. Our calculated enthalpy of formation for ClOOCl from the slope of the van't Hoff plot is in excellent agreement with the recommended value (Burkholder et al., 2015).

The current JPL-recommended error bounds for the ClO-ClOOCl equilibrium constant are large (Burkholder et al., 2015), exceeding 50% at 200 K. The excellent correspondence between the K_{eq} results from this work and Hume et al. (2015) lends confidence to the established parameterization of the JPL data evaluation (Burkholder et al., 2015), suggesting that prescribed error intervals for this reaction can be reduced.

Author contributions. JEK and DMW designed, constructed, and operated the experiment and analyzed and reported the data described in this work.

Competing interests. The authors declare no competing financial interest.

Acknowledgements. We gratefully acknowledge funding from the National Aeronautics and Space Administration (NASA) through grants: NNX15AF60G, NNX15AD87G, and 80NSSC18K1063. We thank Marco Rivero and Norton Allen for engineering support.

References

- Avallone, L. M. and Toohey, D. W.: Tests of halogen photochemistry using in situ measurements of ClO and BrO in the lower polar stratosphere, *J. Geophys. Res.-Atmos.*, 106, 10 411 – 10 421, <https://doi.org/10.1029/2000JD900831>, 2001.
- Boakes, G., Hindy Mok, W. H., and Rowley, D. M.: Kinetic studies of the ClO + ClO association reaction as a function of temperature and pressure, *Phys. Chem. Chem. Phys.*, 7, 4102 – 4113, <https://doi.org/10.1039/B510308H>, 2005.
- Bröske, R. and Zabel, F.: Thermal decomposition of ClOOCl, *J. Phys. Chem. A*, 110, 3280 – 3288, <https://doi.org/10.1021/jp0550053>, 2006.
- Burkholder, J. B., Sander, S. P., Abbatt, J. P. D., Barker, J. R., Huie, R. E., Kolb, C. E., Kurylo, M. J., Orkin, V. L., Wilmouth, D. M., and Wine, P. H.: Chemical kinetics and photochemical data for use in atmospheric studies, evaluation no. 18, JPL Publication 15-10, Jet Propulsion Laboratory, Pasadena, 2015.
- Canty, T. P., Salawitch, R. J., and Wilmouth, D. M.: The kinetics of the ClOOCl catalytic cycle, *J. Geophys. Res.-Atmos.*, 121, 13 768 – 13 783, <https://doi.org/10.1002/2016JD025710>, 2016.
- Cox, R. A. and Hayman, G. D.: The stability and photochemistry of dimers of the ClO radical and implications for Antarctic ozone depletion, *Nature*, 332, 796 – 800, <https://doi.org/10.1038/332796a0>, 1988.
- Ellermann, T., Johnsson, K., Lund, A., and Pagsberg, P.: Kinetics and equilibrium constant of the reversible reaction $\text{ClO} + \text{ClO} + \text{M} \rightleftharpoons \text{Cl}_2\text{O}_2 + \text{M}$ at 295 K, *Acta Chem. Scand.*, 49, 28 – 35, <https://doi.org/10.3891/acta.chem.scand.49-0028>, 1995.
- Ferracci, V. and Rowley, D. M.: Kinetic and thermochemical studies of the $\text{ClO} + \text{ClO} + \text{M} \rightleftharpoons \text{Cl}_2\text{O}_2 + \text{M}$ reaction, *Phys. Chem. Chem. Phys.*, 12, 11 596 – 11 608, <https://doi.org/10.1039/c0cp00308e>, 2010.
- Horowitz, A., Crowley, J. N., and Moortgat, G. K.: Temperature dependence of the product branching ratios of the ClO self-reaction in oxygen, *J. Phys. Chem.*, 98, 11 924 – 11 930, <https://doi.org/10.1021/j100097a019>, 1994.
- Hume, K. L., Bayes, K. D., and Sander, S. P.: Equilibrium constant for the reaction $\text{ClO} + \text{ClO} \leftrightarrow \text{ClOOCl}$ between 250 and 206 K, *J. Phys. Chem. A*, 119, 4473 – 4481, <https://doi.org/10.1021/jp510100n>, 2015.
- Kromminga, H., Orphal, J., Spietz, P., Voigt, S., and Burrows, J. P.: New measurements of OClO absorption cross-sections in the 325–435 nm region and their temperature dependence between 213 and 293 K, *J. Photoch. Photobio. A*, 157, 149 – 160, [https://doi.org/10.1016/S1010-6030\(03\)00071-6](https://doi.org/10.1016/S1010-6030(03)00071-6), 2003.
- Lien, C.-Y., Lin, W.-Y., Chen, H.-Y., Huang, W.-T., Jin, B., Chen, I.-C., and Lin, J. J.: Photodissociation cross sections of ClOOCl at 248.4 and 266 nm, *J. Chem. Phys.*, 131, 174 301, <https://doi.org/10.1063/1.3257682>, 2009.
- Marić, D. and Burrows, J. P.: Analysis of the UV absorption spectrum of ClO: a comparative study of four methods for spectral computations, *J. Quant. Spectrosc. RA*, 62, 345 – 369, [https://doi.org/10.1016/S0022-4073\(98\)00108-3](https://doi.org/10.1016/S0022-4073(98)00108-3), 1999.
- Marić, D., Burrows, J. P., Meller, R., and Moortgat, G. K.: A study of the UV-visible absorption spectrum of molecular chlorine, *J. Photoch. Photobio. A*, 70, 205 – 214, [https://doi.org/10.1016/1010-6030\(93\)85045-A](https://doi.org/10.1016/1010-6030(93)85045-A), 1993.
- Molina, L. T. and Molina, M. J.: Absolute absorption cross sections of ozone in the 185- to 350-nm wavelength range, *J. Geophys. Res.-Atmos.*, 91, 14 501 – 14 508, <https://doi.org/10.1029/JD091iD13p14501>, 1986.
- Molina, L. T. and Molina, M. J.: Production of chlorine oxide (Cl₂O₂) from the self-reaction of the chlorine oxide (ClO) radical, *J. Phys. Chem.*, 91, 433 – 436, <https://doi.org/10.1021/j100286a035>, 1987.
- Newville, M., Stensitzki, T., Allen, D. B., Rawlik, M., Ingargiola, A., and Nelson, A.: LMFIT: non-linear least-square minimization and curve-fitting for Python, Astrophysics Source Code Library, 2016.

- Nickolaisen, S. L., Friedl, R. R., and Sander, S. P.: Kinetics and mechanism of the chlorine oxide ClO + ClO reaction: pressure and temperature dependences of the bimolecular and termolecular channels and thermal decomposition of chlorine peroxide, *J. Phys. Chem.*, 98, 155 – 169, <https://doi.org/10.1021/j100052a027>, 1994.
- Papanastasiou, D. K., Papadimitriou, V. C., Fahey, D. W., and Burkholder, J. B.: UV absorption spectrum of the ClO dimer (Cl₂O₂) between 200 and 420 nm, *J. Phys. Chem. A*, 113, 13 711 – 13 726, <https://doi.org/10.1021/jp9065345>, 2009.
- Plenge, J., Kühl, S., Vogel, B., Müller, R., Stroh, F., von Hobe, M., Flesch, R., and Rühl, E.: Bond strength of chlorine peroxide, *J. Phys. Chem. A*, 109, 6730 – 6734, <https://doi.org/10.1021/jp044142h>, 2005.
- Sander, S. P. and Friedl, R. R.: Kinetics and product studies of the BrO + ClO reaction: Implications for Antarctic chemistry, *Geophys. Res. Lett.*, 15, 887 – 890, <https://doi.org/10.1029/GL015i008p00887>, 1988.
- 10 Sander, S. P., Friedl, R. R., Ravishankara, A. R., Golden, D. M., Kolb, C. E., Kurylo, M. J., Huie, R. E., Orkin, V. L., Molina, M. J., Moortgat, G. K., and Finlayson-Pitts, B. J.: Chemical kinetics and photochemical data for use in atmospheric studies, evaluation no. 14, JPL Publication 02-25, Jet Propulsion Laboratory, Pasadena, 2003.
- Sander, S. P., Friedl, R. R., Abbatt, J. P. D., Barker, J. R., Burkholder, J. B., Golden, D. M., Kolb, C. E., Kurylo, M. J., Moortgat, G. K., Wine, P. H., Huie, R. E., and Orkin, V. L.: Chemical kinetics and photochemical data for use in atmospheric studies, evaluation no. 17, 15 JPL Publication 10-6, Jet Propulsion Laboratory, Pasadena, 2011.
- Santee, M. L., Sander, S. P., Livesey, N. J., and Froidevaux, L.: Constraining the chlorine monoxide (ClO)/chlorine peroxide (ClOOCl) equilibrium constant from Aura Microwave Limb Sounder measurements of nighttime ClO, *Proc. Natl. Acad. Sci. U. S. A.*, 107, 6588i – 6593, <https://doi.org/10.1073/pnas.0912659107>, 2010.
- Simon, F. G., Schneider, W., Moortgat, G. K., and Burrows, J. P.: A study of the ClO absorption cross-section between 240 and 310 nm and the kinetics of the self-reaction at 300 K, *J. Photoch. Photobio. A*, 55, 1 – 23, [https://doi.org/10.1016/1010-6030\(90\)80014-O](https://doi.org/10.1016/1010-6030(90)80014-O), 1990.
- 20 Stimpfle, R. M., Wilmouth, D. M., Salawitch, R. J., and Anderson, J. G.: First measurements of ClOOCl in the stratosphere: the coupling of ClOOCl and ClO in the Arctic polar vortex, *J. Geophys. Res.-Atmos.*, 109, D03 301, <https://doi.org/10.1029/2003JD003811>, 2004.
- Trolier, M., Mauldin, R. L., and Ravishankara, A. R.: Rate coefficient for the termolecular channel of the self-reaction of chlorine monoxide, *J. Phys. Chem.*, 94, 4896 – 4907, <https://doi.org/10.1021/j100375a027>, 1990.
- 25 von Hobe, M., Groß, J.-U., Müller, R., Hrechanyy, S., Winkler, U., and Stroh, F.: A re-evaluation of the ClO/Cl₂O₂ equilibrium constant based on stratospheric in-situ observations, *Atmos. Chem. Phys.*, 5, 693 – 702, <https://doi.org/10.5194/acp-5-693-2005>, 2005.
- von Hobe, M., Salawitch, R. J., Canty, T., Keller-Rudek, H., Moortgat, G. K., Groß, J.-U., Müller, R., and Stroh, F.: Understanding the kinetics of the ClO dimer cycle, *Atmos. Chem. Phys.*, 7, 3055 – 3069, <https://doi.org/10.5194/acp-7-3055-2007>, 2007.
- Wilmouth, D. M., Hanisco, T. F., Stimpfle, R. M., and Anderson, J. G.: Chlorine-catalyzed ozone destruction: Cl atom production from ClOOCl photolysis, *J. Phys. Chem. A*, 113, 14 099 – 14 108, <https://doi.org/10.1021/jp9053204>, 2009.
- 30 Wilmouth, D. M., Salawitch, R. J., and Canty, T. P.: Stratospheric Ozone Depletion and Recovery, in: Green chemistry: an inclusive approach, edited by Torok, B. and Dransfield, T., chap. 3.3, pp. 177 – 209, Elsevier, 2018.
- WMO: Scientific Assessment of Ozone Depletion: 2014, World Meteorological Organization, Global Ozone Research and Monitoring Project - Report No. 55, WMO, Geneva, 2014.
- 35 Wohltmann, I., Lehmann, R., and Rex, M.: A quantitative analysis of the reactions involved in stratospheric ozone depletion in the polar vortex core, *Atmos. Chem. Phys.*, 17, 10 535, <https://doi.org/10.5194/acp-17-10535-2017>, 2017.

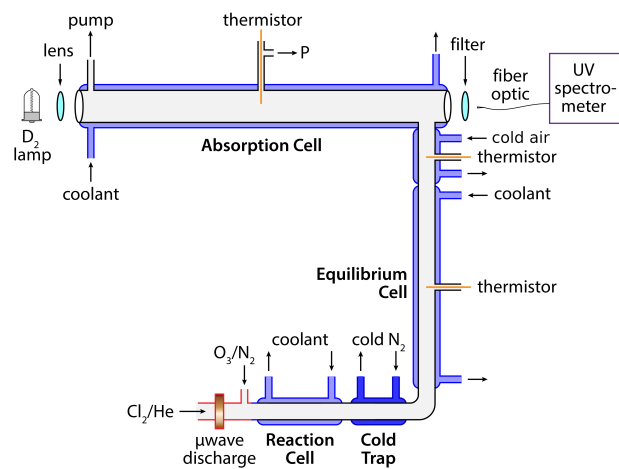


Figure 1. Schematic of the discharge-flow absorbance experiment. Dilute chlorine gas in helium flows through a microwave discharge to form Cl radicals. Dilute ozone in nitrogen is then injected to produce ClO radicals. Self-reaction of ClO occurs in the cold reaction cell to form ClOOC1. When utilized, the cold trap provides for halogen oxide purification. ClO/ClOOC1 equilibrium is established in the equilibrium cell, which is held at the same temperature as the absorption cell. The gas mixture is then characterized via UV spectroscopy in the absorption cell using software developed in-house.

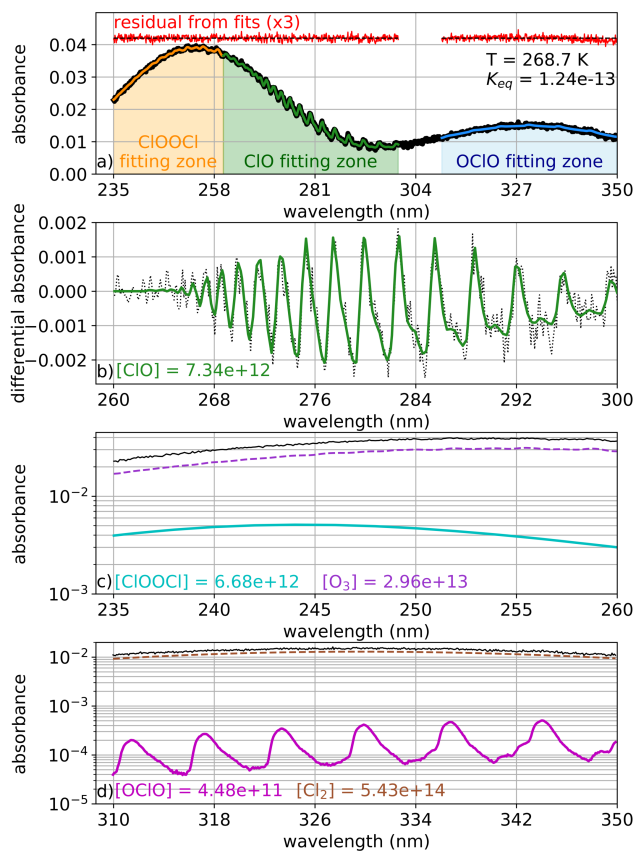


Figure 2. Deconvolution of experimental absorbance spectra to component contributions for an experiment conducted at 268.7 K. (a) Experimental spectrum (black) and the wavelength ranges used for quantification of each spectral component (orange: 235 – 260 nm, green: 260 – 300 nm, blue: 310 – 350 nm). The resulting spectral fits for each region are overlaid on the experimental spectrum in colored traces; the residuals from the fits are plotted in red, magnified by a factor of 3 and offset for clarity. The obtained K_{eq} ($\text{cm}^3 \text{ molecule}^{-1}$) is indicated in the top right corner. (b) Quantification of ClO by the high pass filtration method. The differential absorbance spectrum appears as black dots, and the fitted ClO component is depicted in solid green. (c) Quantification of ClOOC1 (cyan) and O_3 (purple) with the experimental spectrum shown for reference (black). (d) Quantification of OC1O (magenta) and Cl_2 (brown) with the experimental spectrum shown for reference (black). Note that only the primary absorbing species are shown in panels (c) and (d), but all relevant absorbers are included in the fits. Fitted concentrations (molecules cm^{-3}) are given for various component gases.

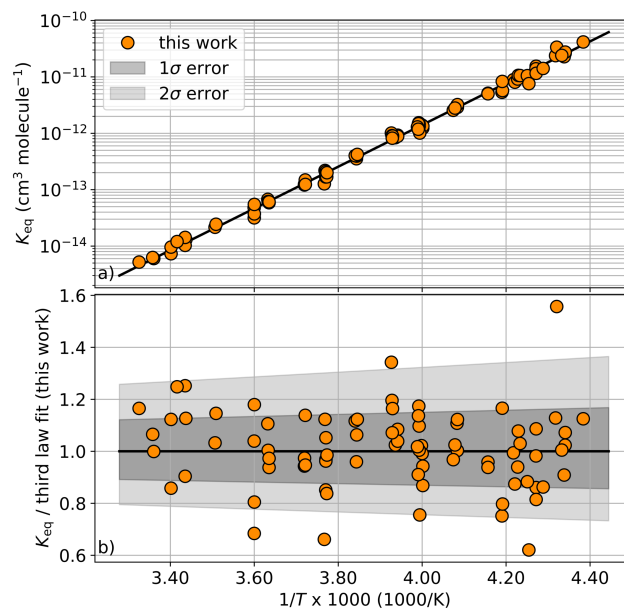


Figure 3. (a) Experimental K_{eq} values as a function of $1000/T$. The black trace is a third law fit of the orange circles, $K_{\text{eq}} = 2.16 \times 10^{-27} e^{(8527 \text{ K}/T)} \text{ cm}^3 \text{ molecule}^{-1}$. Individual values are enumerated in Table 1. (b) Ratio of experimental K_{eq} values to the third law fit. Dark gray shading encompasses the total estimated 1σ error from this study and light shading encompasses the 2σ error.

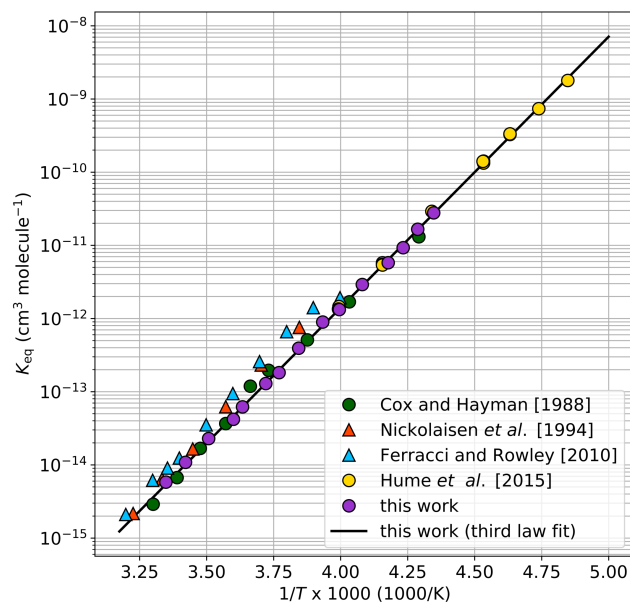


Figure 4. K_{eq} values as a function of $1000/T$. The black trace is the third law fit as determined in Figure 3, $K_{eq} = 2.16 \times 10^{-27} e^{(8527 \text{ K}/T)}$ $\text{cm}^3 \text{ molecule}^{-1}$. For clarity, data from this work are plotted as 3 K averages (purple circles) of the full data set shown in Figure 3. The colored markers are K_{eq} values from prior laboratory studies as reported in the literature.

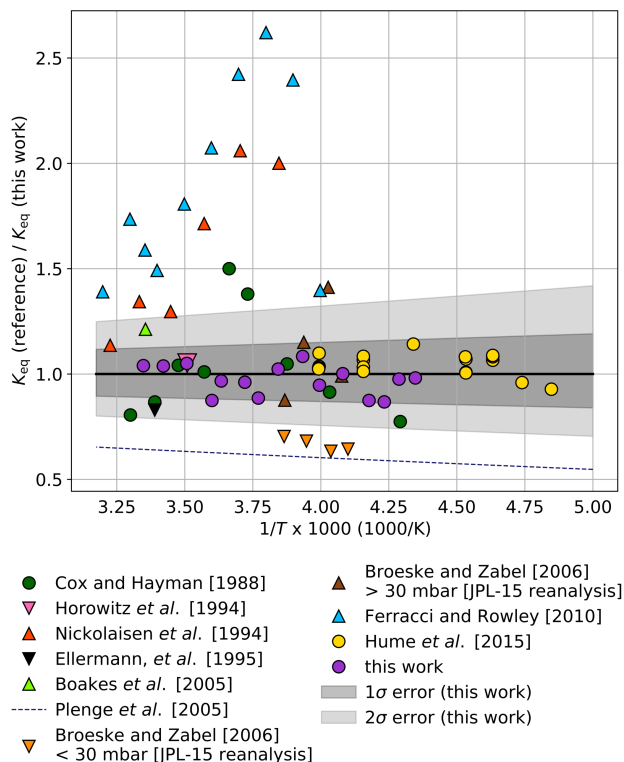


Figure 5. Ratio of K_{eq} values from prior laboratory studies to K_{eq} determined in this work ($K_{\text{eq}} = 2.16 \times 10^{-27} e^{(8527 \text{ K}/T)} \text{ cm}^3 \text{ molecule}^{-1}$) as a function of $1000/T$. Circles indicate studies in which K_{eq} was measured with UV spectroscopy of equilibrium mixtures, while triangles indicate works in which K_{eq} was determined from individual reaction kinetic rates. For clarity, data from this work are plotted as 3 K averages (purple circles) of the full data set shown in Figure 3. Dark gray shading encompasses the total estimated 1σ error from this study and light shading encompasses the 2σ error.

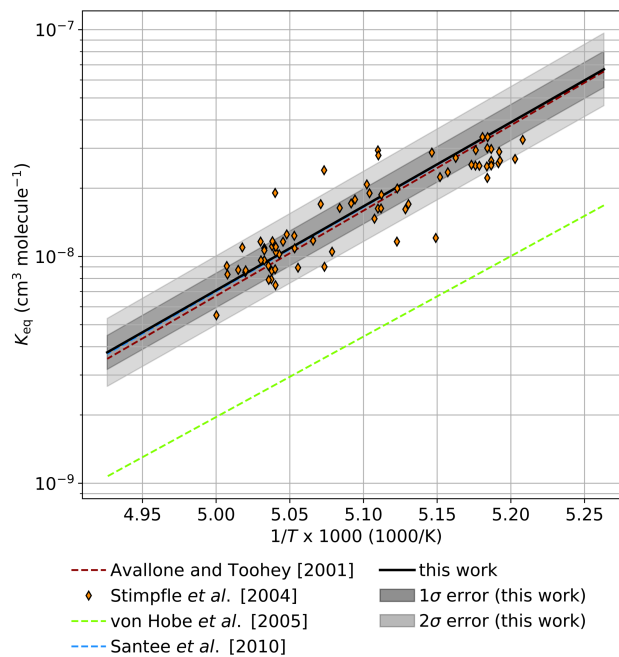


Figure 6. Comparison of extrapolated K_{eq} values from the third law fit in this work ($K_{\text{eq}} = 2.16 \times 10^{-27} e^{(8527 \text{ K}/T)} \text{ cm}^3 \text{ molecule}^{-1}$) to atmospheric observations. K_{eq} (solid black) and error boundaries (gray shaded regions) determined in this study are extrapolated to the temperature range of 190 – 203 K. Expressions for K_{eq} derived from previous atmospheric measurements are presented as dashed lines. Observations of $[\text{ClOOCl}] / [\text{ClO}]^2$ from the nighttime ER-2 flight on 3 Feb 2000 in the SOLVE/THESEO mission out of Kiruna, Sweden are indicated as orange diamonds.

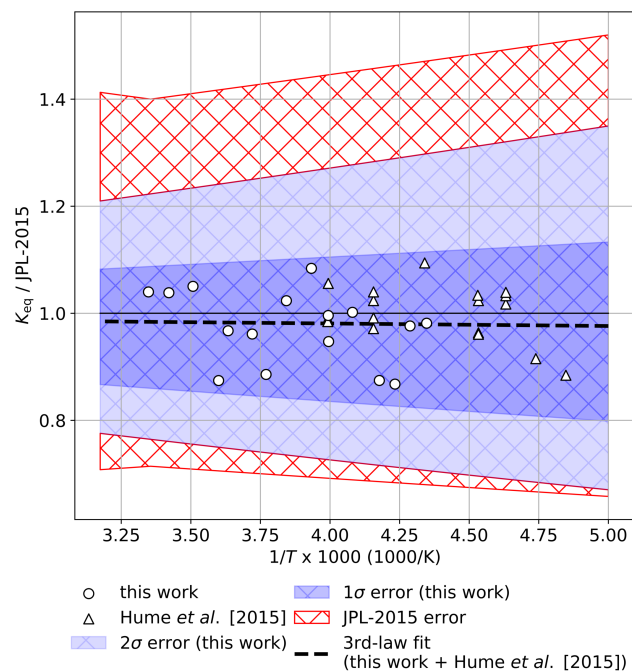


Figure 7. Ratio of a weighted third law fit of K_{eq} (black dashed line) determined from a combination of this work (circles) and Hume et al. (2015) (triangles) to the JPL compendium recommended value (Burkholder et al., 2015). For clarity, data points from this work are plotted as 3 K averages of the full data set shown in Figure 3. Error intervals as reported in this work (darker blue = 1σ , lighter blue = 2σ) and as recommended by JPL-2015 (red cross hatch).

Table 1. Experimental conditions^a, concentrations from spectral deconvolution^b, and K_{eq} values^c

T (K)	$\frac{[ClO]}{10^{11}}$	$\frac{[ClOCl]}{10^{11}}$	$\frac{[OClO]}{10^{11}}$	K_{eq}	T (K)	$\frac{[ClO]}{10^{11}}$	$\frac{[ClOCl]}{10^{11}}$	$\frac{[OClO]}{10^{11}}$	K_{eq}
300.7	244 (0.3)	30.9 (13)	27.3 (0.01)	5.19e-15	253.7	41.2 (2)	158 (5)	—	9.31e-13
297.8	128 (0.4)	10.3 (9)	15.2 (1)	6.29e-15	250.7	43.3 (1)	244 (2)	—	1.30e-12
297.6	127 (0.4)	9.77 (8)	16.3 (0.5)	6.06e-15	250.6	36.2 (2)	154 (1)	—	1.18e-12
294.0	126 (0.4)	11.7 (7)	16.3 (0.5)	7.37e-15	250.6	41.2 (2)	251 (3)	—	1.48e-12
294.0	126 (0.3)	15.4 (6)	15.3 (1)	9.70e-15	250.5	39.7 (2)	243 (2)	—	1.54e-12
292.7	140 (0.2)	23.6 (6)	14.4 (1)	1.20e-14	250.4	25.0 (4)	90.7 (8)	—	1.45e-12
291.1	132 (0.3)	17.9 (10)	15.6 (0.6)	1.03e-14	250.4	23.7 (4)	74.7 (1)	—	1.33e-12
291.1	133 (0.3)	25.3 (8)	15.6 (0.8)	1.43e-14	250.4	26.8 (2)	72.5 (1)	—	1.01e-12
291.0	133 (0.3)	22.7 (3)	16.7 (0.8)	1.28e-14	250.1	37.4 (2)	198 (5)	—	1.42e-12
285.2	124 (0.3)	33.3 (6)	13.6 (1)	2.17e-14	250.0	35.0 (1)	171 (2)	—	1.40e-12
285.0	120 (0.3)	35.4 (5)	13.7 (2)	2.46e-14	249.9	36.0 (2)	160 (6)	—	1.23e-12
277.8	88.4 (0.6)	37.6 (7)	7.56 (3)	4.81e-14	249.9	35.1 (1)	165 (5)	—	1.34e-12
277.8	86.2 (0.7)	23.5 (3)	8.41 (1)	3.16e-14	245.4	31.7 (2)	258 (2)	—	2.57e-12
277.8	90.1 (0.5)	30.3 (5)	8.78 (2)	3.73e-14	245.2	29.7 (2)	246 (2)	—	2.79e-12
277.8	92.6(0.6)	47.0 (2)	7.66 (3)	5.48e-14	244.9	29.9 (2)	282 (3)	—	3.15e-12
275.3	109 (0.4)	80.8 (2)	8.50 (1)	6.80e-14	244.9	31.5 (2)	285 (3)	—	2.87e-12
275.2	108 (0.3)	72.4 (10)	8.41 (2)	6.21e-14	244.9	28.7 (2)	266 (3)	—	3.23e-12
275.1	110 (0.3)	71.1 (8)	7.59 (2)	5.88e-14	240.6	26.8 (3)	367 (1)	—	5.11e-12
275.1	109 (0.4)	72.3 (5)	7.65 (3)	6.09e-14	240.6	27.1 (2)	368 (3)	—	5.01e-12
268.8	77.2 (0.6)	72.2 (8)	4.15 (4)	1.21e-13	238.7	17.5 (4)	164 (3)	—	5.36e-12
268.8	74.7 (0.6)	70.0 (9)	3.87 (6)	1.25e-13	238.6	7.88 (4)	51.8 (11)	—	8.34e-12
268.7	73.8 (0.8)	81.1 (9)	4.54 (3)	1.49e-13	238.6	18.0 (5)	185 (3)	—	5.71e-12
268.7	73.4 (0.6)	66.8 (9)	4.48 (4)	1.24e-13	237.1	6.49 (7)	37.6 (18)	—	8.93e-12
265.5	78.5 (0.5)	78.4 (7)	2.82 (5)	1.27e-13	236.9	7.38 (8)	44.0 (18)	—	8.08e-12
265.3	76.7 (0.5)	129 (6)	3.11 (5)	2.19e-13	236.5	15.1 (4)	210 (2)	—	9.21e-11
265.2	109 (0.8)	202 (2)	—	1.70e-13	236.5	14.5 (6)	223 (4)	—	1.06e-11
265.2	111 (0.8)	236 (5)	—	1.92e-13	236.2	15.0 (4)	238 (4)	—	1.06e-11
265.2	78.1 (0.6)	117 (7)	2.26 (6)	1.92e-13	235.3	10.3 (4)	112 (4)	—	1.06e-11
265.2	77.8 (0.6)	127 (6)	2.15 (8)	2.10e-13	235.1	21.2 (4)	342 (3)	—	7.61e-12
265.1	106 (0.8)	189 (5)	—	1.68e-13	234.1	13.6 (3)	259 (1)	—	1.40e-11
265.0	104 (0.8)	216 (2)	1.17 (25)	2.00e-13	234.1	15.3 (4)	286 (3)	—	1.22e-11
260.4	56.0 (0.9)	126 (4)	1.19 (14)	4.02e-13	234.1	14.2 (4)	310 (3)	—	1.54e-11
260.2	55.6 (1)	110 (5)	1.43 (8)	3.56e-13	234.1	15.6 (3)	283 (2)	—	1.16e-11
260.1	54.1 (0.9)	115 (6)	1.09 (9)	3.93e-13	233.2	7.38 (6)	77.1 (6)	—	1.42e-11
260.0	53.4 (0.9)	120 (5)	1.02 (8)	4.21e-13	231.6	12.4 (4)	366 (2)	—	2.38e-11

Table 1 is continued on the next page.

Table 1. Experimental conditions^a, concentrations from spectral deconvolution^b, and K_{eq} values^c

T (K)	$\frac{[\text{ClO}]}{10^{11}}$	$\frac{[\text{ClOOC}]}{10^{11}}$	$\frac{[\text{OCIO}]}{10^{11}}$	K_{eq}	T (K)	$\frac{[\text{ClO}]}{10^{11}}$	$\frac{[\text{ClOOC}]}{10^{11}}$	$\frac{[\text{OCIO}]}{10^{11}}$	K_{eq}
254.7	45.7 (2)	211 (4)	—	1.01e-12	231.4	10.9 (3)	400 (2)	—	3.37e-11
254.6	47.7 (2)	207 (4)	—	9.10e-13	230.8	12.3 (6)	365 (2)	—	2.41e-11
254.5	45.6 (1)	170 (4)	—	8.18e-13	230.5	10.4 (6)	246 (3)	—	2.27e-11
254.5	44.5 (1)	178 (4)	—	8.99e-13	230.4	7.18 (7)	135 (5)	—	2.62e-11
254.0	44.6 (2)	166 (4)	—	8.35e-13	230.4	7.92 (7)	173 (2)	—	2.76e-11
253.7	43.1 (2)	165 (3)	—	8.88e-13	228.1	5.36 (6)	120 (7)	—	4.18e-11

^aExperimental Pressures: T > 292 K, P = 100 mbar; 280 K < T < 292 K, P = 133 mbar; 270 K < T < 280 K, P = 166 mbar; 261 K < T < 270 K, P = 200 mbar; 252 K < T < 261 K, P = 233 mbar; 242 K < T < 252 K, P = 266 mbar; T < 242 K, P = 333 mbar

^bConcentration units are molecules cm^{-3} . Dashes indicate quantity below limit of detection. Parenthetical values provide % uncertainty in concentration from the spectral deconvolution.

^c K_{eq} units are $\text{cm}^3 \text{ molecule}^{-1}$.